

Applied and theoretical considerations for constructing spatially explicit individual-based models of marine larval fish that include multiple trophic levels

Albert J. Hermann, Sarah Hinckley,
Bernard A. Megrey, and Jeffrey M. Napp



Hermann, A. J., Hinckley, S., Megrey, B. A., and Napp, J. M. 2001. Applied and theoretical considerations for constructing spatially explicit individual-based models of marine larval fish that include multiple trophic levels. – ICES Journal of Marine Science, 58: 1030–1041.

Individual-based modelling (IBM) techniques offer many advantages for spatially explicit modelling of marine fish early life history. However, computationally efficient methods are needed for incorporating spatially explicit circulation and prey dynamics into IBMs. Models of nutrient–phytoplankton–zooplankton (NPZ) dynamics have traditionally been formulated in an Eulerian (fixed spatial grid) framework, as opposed to the pseudo-Lagrangian (individual-following) framework of some IBMs. We describe our recent linkage of three models for the western Gulf of Alaska: (1) a three-dimensional, eddy-resolving, wind- and runoff-driven circulation model, (2) a probabilistic IBM of growth and mortality for egg and larval stages of walleye pollock (*Theragra chalcogramma*), and (3) an Eulerian, stage-structured NPZ model which specifies production of larval pollock prey items. Individual fish in the IBM are tracked through space using daily velocity fields generated from the hydrodynamic model, along with self-directed vertical migrations of pollock appropriate to each life stage. The NPZ dynamics are driven by the same velocity, temperature, and salinity fields as the pollock IBM, and provide spatially and temporally varying prey fields to that model. The resulting prey fields yield greater variance of individual fish attributes (e.g. length), relative to models with spatially uniform prey. Practical issues addressed include the proper time filtering and storage of circulation model output for subsequent use by biological models, and use of different spatial grids for physical and biological dynamics. We demonstrate the feasibility and computational costs of our coupled approach using specific examples from the western Gulf of Alaska.

Keywords: biophysical models, individual-based models, recruitment, spawning.

Published electronically 14 August 2001.

A. J. Hermann: Joint Institute for the Study of the Atmosphere and the Oceans, University of Washington, Seattle, WA 98115, USA; tel: +1 206 526 6495; fax: +1 206 526 6485; e-mail: hermann@pmel.noaa.gov. S. Hinckley, B. A. Megrey, and Jeffrey M. Napp: NOAA, National Marine Fisheries Service, Seattle, WA 98115, USA. Correspondence to A. J. Hermann.

Introduction

Fisheries research continues to establish important linkages among fish populations, their prey and predators, and characteristics of the immediate physical environment (e.g. circulation, temperature). As interactions among populations and the environment are clarified by field measurements and laboratory experiments, there is a growing need for models that simultaneously include several trophic levels and specific populations. A single modelling approach may not serve well for all components.

The majority of marine ecosystem models are formulated in terms of the aggregate properties of each model component, e.g. the mean biomass of phytoplankton per unit volume or the mean number of fish per unit area. In effect, such models follow the evolution of the “mean individual” of a population through time. An increasingly popular class of population models, commonly referred to as “individual-based” models (IBM), keeps track of distinct individuals within a population, each of which interacts with other individuals and its physical environment based on its present state and possibly its past history. Such models are frequently stochastic in

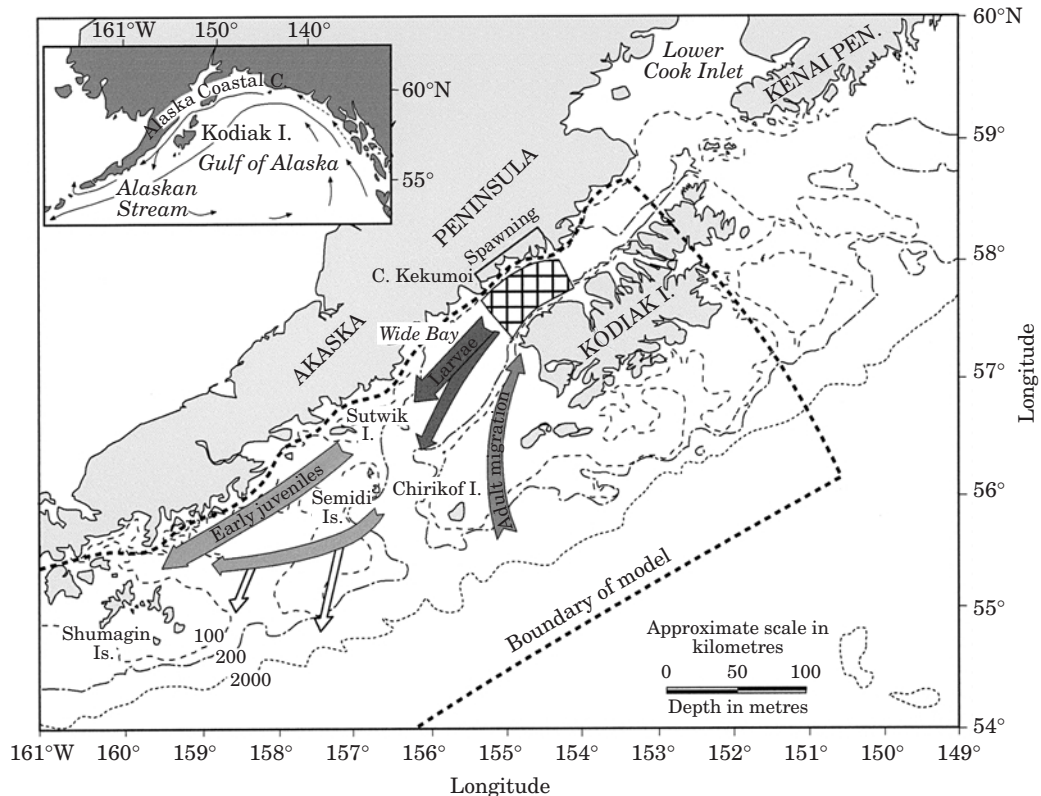


Figure 1. Summary of early life history for walleye pollock spawning at the exit of Shelikof Strait. Primary regional currents are shown inset. Subsequent to spawning, hatched larvae from eggs drift southwest with the Alaska Coastal Current; some are transported up onto the shallow, near-coastal shelf area while others are transported out into the deeper waters of the Alaskan Stream. Dashed line indicates the boundary of the finely resolved physical model domain (~4-km mean spacing).

design. Recent examples include DeAngelis *et al.* (1991), Rose *et al.* (1993), Crowder *et al.* (1993), Werner *et al.* (1993, 1996), and Hinckley *et al.* (1996). Continuing developments in computer speed and architecture have rendered the IBM approach to fisheries modelling increasingly tractable.

Realistic population or ecosystem modelling may require explicit treatment of spatial history. Many marine species spend their life stages in different physical environments (e.g. separation between spawning grounds, nurseries and adult feeding areas). Even for species with no appreciable horizontal transport, vertical migration through light, temperature, and prey concentration gradients can play a significant role in determining growth and survival.

We consider the simultaneous inclusion of circulation and prey fields in a spatially explicit, three-dimensional IBM for walleye pollock (*Theragra chalcogramma*) near Shelikof Strait, Alaska. An overview of the area and the life history of pollock spawning in Shelikof Strait are shown in Figure 1. Its early life history has been studied extensively by the Fisheries Oceanography Coordinated Investigations (FOCI) programme (Schumacher and

Kendall, 1995; Kendall *et al.*, 1996). Spawning eggs develop into larvae and juveniles as they are advected to the southwest with the prevailing currents. To capture the early life history, the models include passive advection and active vertical locomotion of individual fish through their habitat and feeding on prey items whose concentration varies in space and time.

We use three linked complex models, each designed to address issues relevant to pollock life history near Shelikof Strait:

(1) The three-dimensional, eddy resolving, semi-spectral primitive equation circulation model (SPEM) of Haidvogel *et al.* (1991), adapted to the region by Hermann and Stabeno (1996), is capable of describing both the mean flow and much of its horizontal and vertical complexity. Forcing includes twice-daily geostrophic winds, suitably rotated to account for the ageostrophic effects of coastal topography (Stabeno *et al.*, 1995) and coastal run-off (Royer, 1982). Results have been calibrated using current meter and drogued drifter data (Stabeno and Hermann, 1996).

(2) The stochastic, spatially explicit IBM of walleye pollock (Figure 2) described by Hinckley *et al.* (1996)

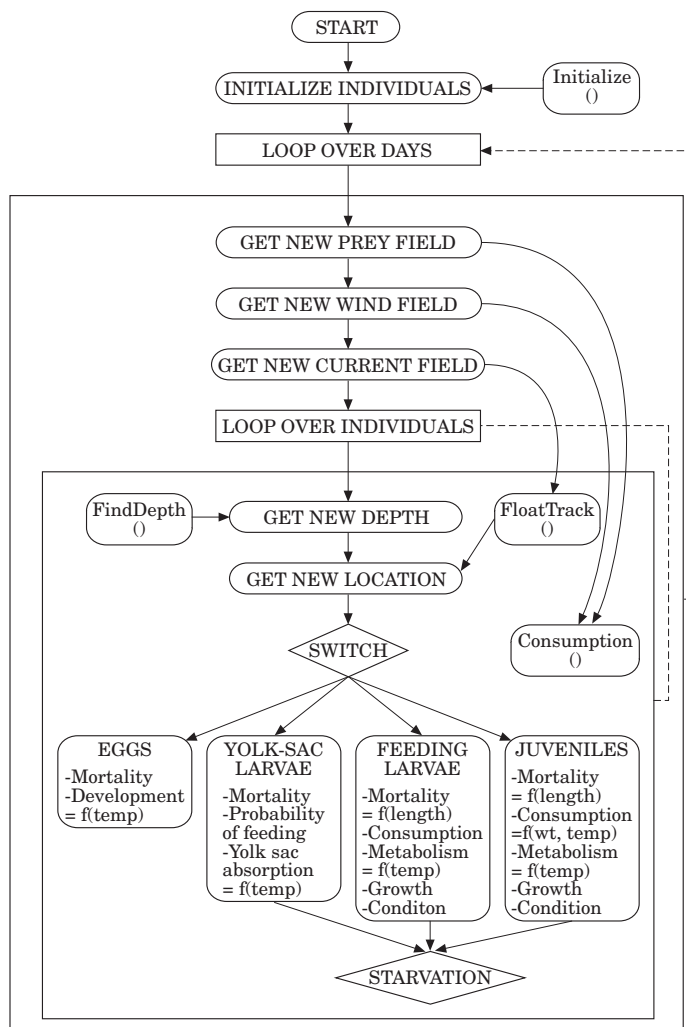


Figure 2. Flowchart of the individual-based model structure for walleye pollock.

tracks individuals through time and space, and models life-stage specific processes such as development, feeding, growth, and mortality. The model follows individuals through the egg, yolk-sac, feeding larval, and juvenile stages from late winter to the fall of their first year. As discussed in [Hinckley et al. \(1996\)](#), the use of a stochastic model results in more realistic length distributions than a deterministic model, and significantly impacts the spatial distribution of the population. The IBM now includes prey selection based on stage and size of pollock, and the effects of turbulence on feeding ([Megrey and Hinckley, this volume](#)). Output from an earlier version of this model compared favourably with larval surveys spanning several years ([Hermann et al., 1996](#)).

(3) The three-dimensional nutrient–phytoplankton–zooplankton (NPZ) model ([Figure 3](#)) is a deterministic, lower trophic level model similar to that described in

[Frost \(1987, 1993\)](#) and is formulated on a fixed spatial grid. The model follows total nitrogen and phytoplankton concentrations in a three-layered water column consisting of a mixed layer, a stratified layer, and an underlying source layer. Of the herbivores included, *Neocalanus* spp. is the mesozooplankton biomass-dominant ([Napp et al., 1996](#); [Incze et al., 1997](#)), acting to consume the bulk of primary production, and *Pseudocalanus* spp. is the prey resource for larval pollock ([Kendall et al., 1987](#); [Nakatani and Maeda, 1987](#); [Hillgruber et al., 1995](#)). Stages of *Pseudocalanus*, from egg to adult, are followed separately. Model equations as well as comparisons to data and an optimization analysis are available in [Hinckley \(1999\)](#).

Both biological models receive input from the circulation model in the form of currents, temperature, and salinity ([Figure 4](#)). The IBM also uses wind data directly to calculate effective turbulence levels at larval depths

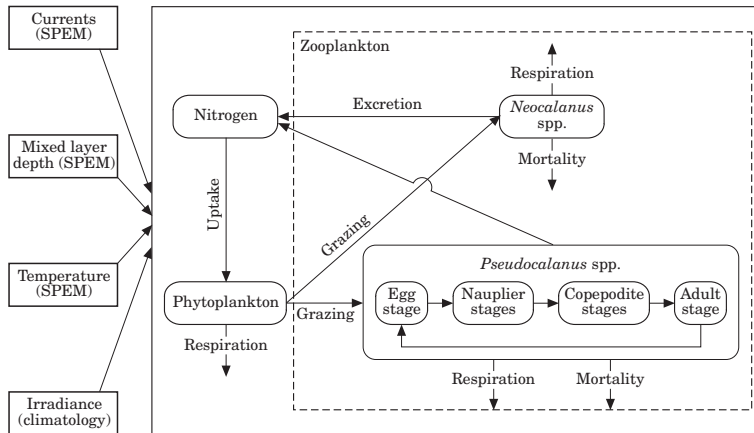


Figure 3. Flowchart of the nutrient-phytoplankton-zooplankton (NPZ) model (*Pseudocalanus* spp. stages: egg, six naupliar stages, five copepodite stages, and adult).

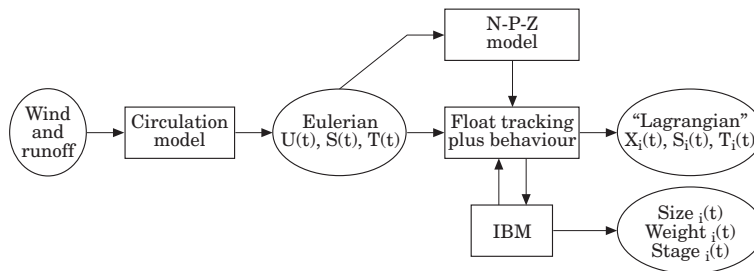


Figure 4. Summary of coupling among the three models.

through the empirical formula of [MacKenzie and Leggett \(1993\)](#). Irradiance derived from climatological means and mixed layer depths derived from the SPEM model are input to the NPZ model.

We discuss applied and theoretical issues relevant to coupling the Lagrangian biological (IBM), Eulerian physical (SPEM), and Eulerian biological (NPZ) models, and describe our present coupling techniques. Relevant coupling issues include: the use of time-filtered versus unfiltered circulation fields for tracking individuals, the choice of a time step for updating individual positions, the use of different spatial grids for biological and physical models, and the choice of spatial boundary conditions for each model. Issues relevant to coupling the IBM with SPEM receive the most extensive treatment, as we have the longest experience with these two models. We then describe results of float-tracking experiments using SPEM output, which bear directly on coupling issues, and results from the NPZ model driven by SPEM velocities, and their effect when used as prey fields for the IBM. Finally, we summarize computational and storage requirements for the models as currently implemented.

Materials and methods

Methods for coupling Lagrangian and Eulerian models

Spatially explicit biological models may be constructed using either Eulerian or Lagrangian frames of reference, a distinction drawn by other plankton modelers (e.g. [Lande and Lewis, 1989](#)). An Eulerian biophysical model is here defined as one that follows the evolution of some quantity at discrete, fixed physical locations. Typically, these locations are the fixed grid points used by a numerical model, although analytical solutions throughout the domain are sometimes possible for simple Eulerian models. Changes in any quantity are due not only to local biological processes, but also to advective and diffusive exchange with adjacent locations, e.g.:

$$B[\underline{x}, t] = -\underline{u}[\underline{x}, t] \cdot \nabla B[\underline{x}, t] + \nabla \cdot (\underline{k} \nabla B) + f_E[B, \underline{x}, t], \quad (1)$$

where B represents the modeled quantity, $\underline{u}=(u,v,w)$ is the fluid velocity, \underline{k} represents horizontal and vertical eddy diffusion coefficients, $\underline{x}=(x,y,z)$ is the spatial

location, t is time, and f_E represents changes due to biological processes (birth, growth, death, etc.) at a fixed location.

In the hydrodynamic literature, a Lagrangian reference frame is one which moves with a discrete parcel of fluid. By extension, we may define a Lagrangian biological model as one that follows an individual organism or group of organisms moving through space as it is advected by the ambient currents. Mathematically we represent changes following an individual (or group) i as:

$$DB_i/dt = f_L(B_i[t], x_i[t], t) \quad (2)$$

where:

$$x_i[t] = \int_0^t u_i(x_i[t'], t') dt' \quad (3)$$

where $B_i(t)$ represents some property of the individual (or group) at time t , $x_i(t) = (x_i[t], y_i[t], z_i[t])$ represents the spatial path through time, and f_L represents any non-conservative changes due to biological processes. Such changes may include processes based on past history. The quantity u_i represents each component of the fluid velocity u plus any directed motions, such as vertical migration owing to buoyancy or locomotion. Note the potentially "individual-based" nature of the Lagrangian model, though in fact such models need not be IBMs *per se*.

Here, we choose to use an IBM for young pollock, an Eulerian NPZ model to generate prey fields, and an Eulerian physical model (SPEM) to generate velocity, salinity, and temperature fields for both.

IBM-SPEM coupling

At its core, our Lagrangian problem is one of accurately tracking an individual in a time and space variable, partially unknown environment. When a hindcast of a population for a specific time period is attempted, we must consider both the accuracy of the hindcast velocity field and the accuracy of the scheme used for tracking individuals within that velocity field. Both the physical and biological environment experienced by the tracked individuals (in particular, the prey field they experience) may be strongly affected by these factors.

The Navier-Stokes equations that form the basis of hydrodynamic models are an exact representation of the fluid evolution, but can never be solved exactly (that is, at arbitrarily high spatial and temporal resolution) on any finite computer. Nonetheless, hydrodynamic models have achieved some success in resolving both large-scale and, to a lesser extent, mesoscale (~ 10 km) velocity features of coastal and open-ocean environments. Increasingly sophisticated data assimilation schemes

have allowed for ever-more accurate hindcasts and forecasts of velocity fields using these equations when hydrographic and velocity data are available (Fukumori and Malanotte-Rizzoli, 1995). Even when such data are not available, or when the model is not intended as a hindcast, one may wish to reproduce the dynamics of a particular region in some statistical sense; for example, to achieve the correct scale and frequency of passage of eddies and correct mean flows.

Ideally, we wish to use a three-dimensional hydrodynamic model to generate accurate velocity fields through which individuals can be tracked in a stochastic IBM with arbitrarily high spatial and temporal resolution. Several possibilities exist for coupling a circulation model with a stochastic IBM: (i) run the hydrodynamic and individual-based models in parallel, updating individual positions at each new time step of the hydrodynamic model. Run the combined model many times, one run for each realization of the IBM. (ii) Run the hydrodynamic and individual-based models in parallel just once, computing all realizations of the IBM simultaneously. (iii) Run the hydrodynamic model once, tracking a number of passive floats whose initial position corresponds to initial organism concentrations in the model domain. Store the resulting Lagrangian series of position, temperature, salinity, etc. for later use by an IBM without any further spatial tracking [Figure 5(a)]. (iv) Run the hydrodynamic model once, storing all relevant gridded velocity, temperature, and salinity fields at each model grid point and time step for subsequent use by an IBM that performs its own spatial tracking [Figure 5(b)].

All approaches have both advantages and drawbacks. Method (i) is at present computationally prohibitive for most three-dimensional hydrodynamic models, as it requires a potentially large number of runs. Method (ii) reduces computation of the physical model, but requires huge amounts of computer memory to keep track of all biological realizations simultaneously. Method (iii) is efficient and allows for many individuals, but eliminates the possibility of adding individual behaviour (in particular, vertical locomotion), which varies as a function of the individual's unique, partly random, life history. In other words, any realization of the IBM in method (iii) cannot feed back on the float tracks, which are determined by the hydrodynamic model alone. Method (iv) offers the possibility of feedback, but requires potentially huge amounts of data storage to accommodate the three-dimensional circulation model output. Hence we propose a modification of (iv):

(iv-a) Run the hydrodynamic model once, storing suitably low-pass-filtered (high frequencies removed), decimated time-series of all relevant gridded velocity, temperature, and salinity fields at each model grid point for subsequent use by an IBM that performs its own spatial tracking.

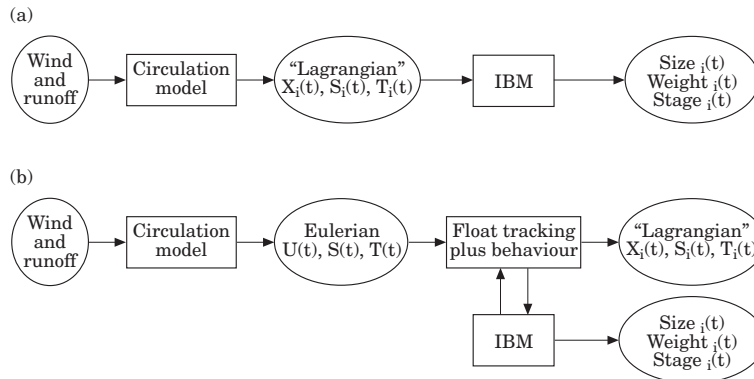


Figure 5. Two schemes for implementing a probabilistic Lagrangian biophysical model of the early life stages of marine fish. (a) scheme (iii); (b) scheme (iv) (see text).

Note that the characteristics of the filter used in (iv-a), and the interval for subsampling, depend on what portion of the full spectrum of motions is considered “expendable” for purposes of spatial tracking. For example, time-filtering would introduce a bias if locomotion of individuals were somehow correlated with higher frequency current fluctuations (e.g. swimming in response to tides or internal waves) that had been removed. In general, primitive equation hydrodynamic model output contains far less energy at superinertial frequencies than is observed in real oceanographic measurements (Stabeno and Hermann, 1996), and such fluctuations that do exist in the model are poorly correlated with the real data. Nevertheless, subsampling without filtering, while partially adequate for spatial tracking, could lead to serious aliasing errors when much high frequency energy is present. We suggest filtering to eliminate this poorly correlated high frequency band, but retain significantly correlated sub-inertial motions. The significance of tides is context-dependent and needs to be considered carefully.

Consider how spatial tracking in method (iv-a) might be efficiently accomplished with the filtered fields, and whether any of the information lost in the filtering process might be added back in by the tracking algorithm. Neutrally buoyant floats have been tracked in many numerical ocean models. Instantaneous float velocities are generally derived by interpolating between grid points to the current location of each float. Generally, the floats are advanced in time using the same time step as is used for solving the governing hydrodynamic equations, but this need not be the case, and especially not in our situation where previously stored, filtered velocity fields are used. How, then, do we choose a time step for float tracking that is sufficiently short but not computationally prohibitive? One requirement is that the Lagrangian decorrelation time T_L be much longer than the time step dt used for float tracking:

$$T_L \gg \Delta t \tag{4}$$

The property T_L is defined as follows. When moving within a turbulent flow field, particle velocities eventually become decorrelated from their starting velocities. This loss of “memory” can be characterized by the integral of the lagged correlation function:

$$T_L = \int_0^{\infty} R(r) dr \tag{5}$$

where

$$R(t) = (1/u'u') \left[(1/T_{max}) \int_0^{T_{max}} u'_i(t)u'_i(t+r) dr \right], \tag{6}$$

where $u'u'$ is the mean turbulent kinetic energy of the flow, $u'_i(t)$ is the velocity of the particle i at time t , T_{max} is a suitably long time used for averaging and the square brackets denote an ensemble mean over all particles.

When (4) is satisfied, the moving float (individual) can be reasonably approximated to travel at constant velocity for a period that is longer than the time between updates of the velocity field used for tracking. When this is not the case, tracks will diverge from “true” particle paths. Haidvogel (1982) has demonstrated that adequate spatial resolution is also crucial for accurate float tracking; with overly coarse resolution, non-linear interactions present in the hydrodynamic equations will be improperly represented and floats will diverge from their true path.

We generally expect time filtering of velocities to increase T_L . This is helpful in allowing a longer time step for tracking, as well as reducing the size of the velocity file, if the higher-frequency variability can be reasonably sacrificed. If tides are a critical aspect of the individual’s life history, there may be no easy way to avoid using unfiltered velocities, and a short tracking time

step. Note, however, that some information about tides could be stored in compact form (amplitude and phase) for later use; such reconstructed tidal velocities could be added to filtered (subtidal) velocity fields directly in the tracking algorithm, potentially reducing storage requirements.

The model used here is a prognostic, rigid-lid, hydrostatic, three-dimensional, primitive equation model of velocity and salinity fields in the northern Gulf of Alaska (Hermann and Stabeno, 1996). Stabeno and Hermann (1996) demonstrated that the model yields realistic mean flows and eddy statistics (frequency of passage of mesoscale eddies) in the vicinity of Shelikof Strait. Tides are not explicitly formulated, but some high-frequency (near-inertial) oscillations are included in the dynamics. Boundary conditions were provided using a telescoped grid with a toroidal, re-entrant channel (Hermann and Stabeno, 1996). The finely resolved portion of the model domain (4-km mean spacing; Figure 1) extends from the entrance of Shelikof Strait to slightly westward of the Shumagin Islands, and southward to just beyond the Alaskan Stream.

NPZ-SPEM coupling

The characteristic length and time scales of biological properties are strongly influenced by, but not identical to, the corresponding scales of their physical environment. Ideally, we would like to resolve both fields so finely in space and time that all relevant scales are included, but this is rarely possible because of the cost involved. As a compromise, we chose different horizontal and vertical scales for the Eulerian physical and biological models. For NPZ dynamics, we generally require a finer vertical scale than for the physical model owing to the sensitivity of primary production to changes in mixed layer depth (MLD). In particular, we wish to resolve the vertical dimension finely enough for small changes in MLD (here externally supplied) to trigger blooms at the appropriate time (e.g. when MLD becomes less than the critical depth). This entails a sacrifice of horizontal resolution. How crucial this loss may be depends on the relative magnitude of advective change, versus locally (biologically) driven change. The character of mesoscale eddies in the vicinity of Shelikof Strait suggests a horizontal spacing of ~ 12 km as a desirable goal; note, however, that the useful NPZ resolution is fundamentally dependent on the characteristic scales of the modelled circulation, rather than the characteristic (and typically finer) scales of the circulation itself. As a first attempt, we chose to use a model with 1-m resolution in the vertical (coverage 0–100 m), and 20-km resolution ($5 \times$ the physical model) in the horizontal (Figure 6). Background horizontal and vertical diffusivities were set at 10 and $10^{-5} \text{ m}^2 \text{ s}^{-1}$, respectively.

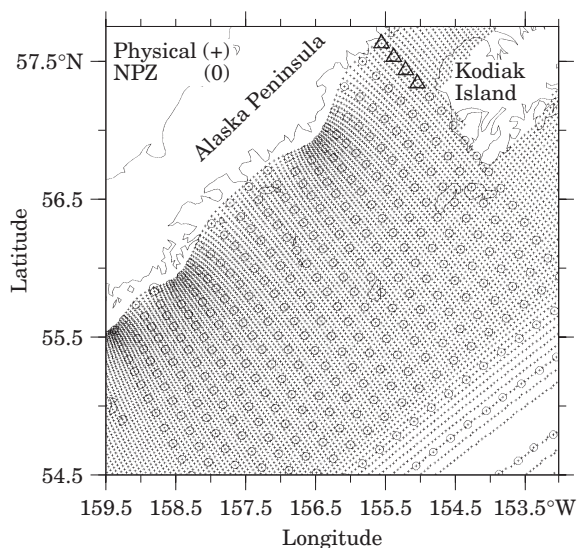


Figure 6. Overlay of SPEM (crosses) and NPZ (circles) model grids. Triangles indicate upstream (inflow) boundary.

As with the IBM, we use time-filtered, stored output from the physical model as input for the NPZ model. Time-filtered barotropic stream-function output from the physical model is subsampled to the NPZ grid. The horizontal gradients of the barotropic stream function, divided by water-column depth (or by 100 m in regions of deeper bathymetry), yields depth-averaged velocities at each horizontal location. These are used to calculate the horizontal divergence and, subsequently, the vertical velocities. This approximation distorts the true vertical shear and vertical velocities, but avoids spurious (and potentially very large) convergence, which typically results from subsampling a full, three-dimensional velocity field. Errors in the computed vertical velocity field are likely not too large in this case; vertical upwelling of nutrients strongly affects production in some parts of the ocean, but in the Gulf of Alaska downwelling predominates during most of the year. Horizontal advection and mixed layer deepening are hence the more significant sources of nutrients to feed production.

The vertical structure of the NPZ model assumes a mixed layer of variable depth with uniform properties, and a stratified region beneath (down to 100 m), where mixing is based on the spatially constant background diffusivity. MLD time-series were generated using the circulation model's density profiles at the horizontal locations of the NPZ grid. A simple algorithm was employed, where MLD was defined as the depth at which the salinity field (the primary determinant of density in this region during spring) assumes a value 0.05 psu greater than the surface value. Clearly, this is a crude parameterization and future circulation modelling will include explicit mixed layer physics.

Since we have used stored, time-filtered, and decimated stream-function fields to drive the NPZ model, the effects of that filtering on the prey dynamics must be considered. Float-tracking experiments suggest an acceptable loss of temporal information for our rigid lid circulation model with no tides (see Results). The effect of varying spatial resolution on the NPZ fields depends on the magnitude of the advection terms, relative to the local non-conservative (biological) dynamics. If biological dynamics predominate over advective change, then coarse resolution of the advective terms is a permissible compromise. We may ultimately be able to invoke spatially dependent diffusivities to partially compensate for the loss of spatial resolution. Biological components with the fastest turnover times (phytoplankton) will be the least susceptible to aliasing from the choice of a coarse spatial grid, while those with longer turnover times will be most affected. Napp *et al.* (1996) have demonstrated that advection plays a large role in determining the spatial patterns of phytoplankton and zooplankton observed in Shelikof Strait. Future iterations of coupled SPEM-NPZ models will examine the consequences of decreasing the spatial scale.

The NPZ model domain is a subset of the physical model, and needs boundary conditions for each of its biological variables. In the interior, the balance of (1) holds; separating out the spatial terms yields:

$$B_i[\underline{x},t] = -\underline{u}^h \cdot \nabla^h B + \nabla^h \cdot (\underline{k}^h \cdot \nabla^h B) - wB_z + (k^z \nabla^z B)_z + f_{\text{biol}} [B, \underline{x}, t] \quad (7)$$

where B is an NPZ model variable (e.g. phytoplankton), ∇^h is the horizontal gradient operator, u^h and k^h are the horizontal velocities and eddy diffusivity, respectively, w is the vertical velocity, k^z is the vertical eddy diffusivity and f_{biol} represents all non-conservative biological dynamics. Perfect knowledge of upstream values would permit direct specification of B at the upstream boundary; instead, we are limited to several springtime measurements per year taken 7 km apart along a transect across the lower exit region of Shelikof Strait (Incze and Ainaire, 1994; Napp *et al.*, 1996; Incze *et al.*, 1997). Hence, we provide values at the upstream end by running the model in one-dimensional mode (no advection or horizontal diffusion):

$$B_i[\underline{x},t] = -wB_z + (k^z \nabla^z B)_z + f_{\text{biol}} [B, \underline{x}, t] \quad (8)$$

Boundary values computed using (8) are advected into the interior, driven by the velocity field and the horizontal gradient term of (7).

At the downstream boundary, a zero gradient condition was imposed for all biological variables ($B_i[\underline{x},t]=0$).

IBM-NPZ coupling

Some of the issues discussed above for the proper application of stored circulation fields to the IBM hold for the application of Eulerian biological fields to the IBM as well. Ideally, we could interpolate perfectly accurate Eulerian prey values onto the location and time of the tracked individuals of the Lagrangian IBM. In practice we must settle for statistically correct prey fields, driven in part by the statistically correct velocity fields from the physical model. The mapping of prey values to individual fish locations is straightforward, and is performed in the IBM using simple linear interpolation of NPZ output in time and space.

The present boundary conditions for the IBM are: (1) when an individual is located outside the NPZ domain, prey values of the NPZ boundary point nearest that individual's present location are applied; (2) when an individual is advected outside the finely resolved circulation model domain, it is removed from the population. We also trap individuals at the downstream (south-western) end of the physical domain, to prevent their re-entrance at the upstream end.

Results

Float-tracking experiments

To address the accuracy of float tracking with pre-stored, filtered, and decimated velocity fields versus direct tracking with the unfiltered field, we present results from a simulation of 1987 currents and float tracks in the Gulf of Alaska (for details of model forcing, see Hermann *et al.*, 1996). Figure 7(a) illustrates the results of float tracking by direct updating (case a) in the hydrodynamic model; that is, ten floats are tracked using the instantaneous velocity produced by the model at each time step (0.0375 h) with a fourth-order Runge-Kutta scheme. Interpolation of velocities between model grid points is performed as described in Hoffmann *et al.* (1989); briefly, this entails linear interpolation in the horizontal and spectral (here, Chebyshev) expansion in the vertical. Initial positions span a northwest-southeast line between the Alaska Peninsula and the northwestern corner of Kodiak Island, at 40-m depth. Many of the floats circulate around and through a cyclonic-anticyclonic eddy pair, just downstream from the exit of Shelikof Strait. Note how some of the floats, released in deep regions, cross bathymetric contours to the shallower continental shelf.

Now consider the same set of floats tracked with pre-stored, filtered, and decimated velocity fields. These fields are produced by applying a cosine-Lanczos 30-h low-pass filter to the original model time series during execution of the run, and storing the filtered result once per day. This filtering process eliminates all of the near-inertial, internal wave oscillations. We wish to see if

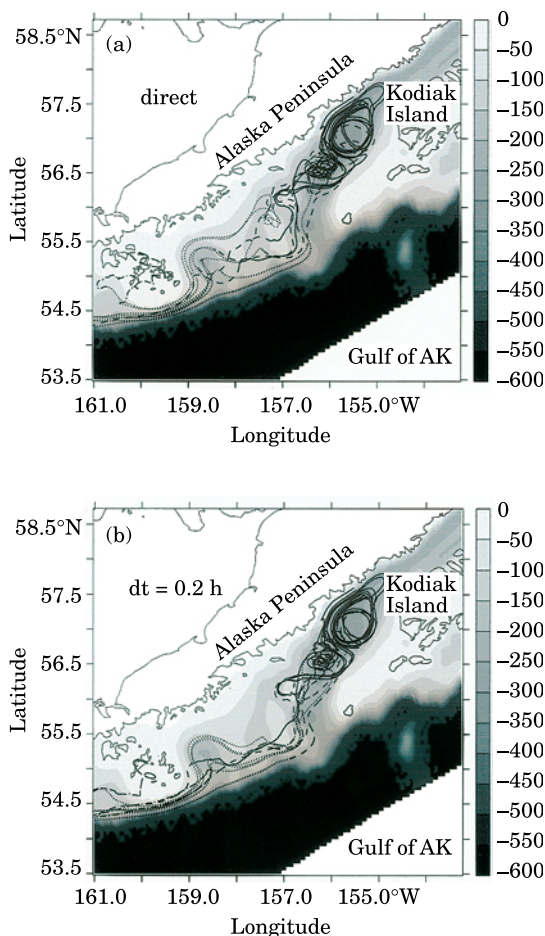


Figure 7. Tracks of ten floats (released along a cross-shelf line at 40 m depth on DOY 135) generated (a) by directly updating float positions at each time step and (b) by updating float positions using previously stored, filtered, daily velocity fields, with $dt=0.2$ h for the float-tracking algorithm (SPEM simulation for 1987). Tracks are coded by time interval: DOY 135–165 (solid); DOY 165–195 (short dashes); DOY 195–225 (broken); DOY 225–255 (dot-dash); DOY 255–270 (long dashes). Model bathymetry (m) is shown in greyscale.

accurate float tracking can be achieved with time steps >0.0375 h of the “direct” unfiltered method, and whether the resulting tracks of the two compare favourably. Float-tracking with pre-stored velocities is attempted with three different values of the time step: (case b) $dt=1$ h; (case c) $dt=0.2$ h; (case d) $dt=0.04$ h. Linear interpolation in time is used to provide velocity values in between the stored daily values; spatial interpolation is performed as in case a. In each case, floats were seeded at exactly the same locations and depths. In case b, the broadly defined paths of the float tracks from case a are reasonably well reproduced, but the details differ as the floats are advected downstream. Can a shorter time step do better? Case c [Figure 7(b)] differs from case b primarily in the improved fit with features in

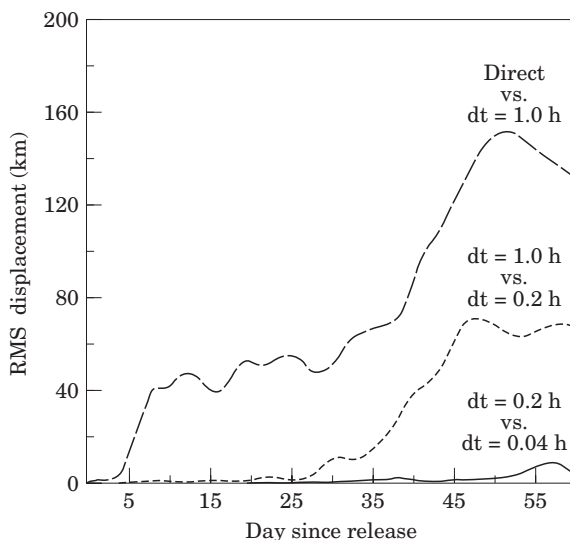


Figure 8. Root-mean-square relative displacement of float tracks among different tracking experiments as a function of time since the start (DOY 105, 1987): dashed line, filtered velocities with $dt=1$ h (case b) versus “direct” tracking (case a); dotted line, $dt=1$ h (case b) versus $dt=0.2$ h (case c); solid line, $dt=0.2$ h (case c) versus $dt=0.04$ h (case d).

the vicinity of the Shumagin Islands. Case d, with highest temporal resolution, exhibits no substantial difference from case c.

The root-mean-squared (rms) horizontal displacement of the floats between cases a and b, b and c, and c and d is plotted in Figure 8. During the first 4 d of simulation, case b generates float tracks within ~ 2 km of their locations in case a. Thereafter, the results diverge to a mean displacement of ~ 40 km (the typical width of the deep strait and sea valley in this area). Near day 30, the mean displacement increases once more, ultimately achieving values of ~ 140 km. Cases b and c diverge significantly from each other after day 30, while cases c and d are essentially identical through day 60.

Apparently, by shortening the time unit from 1 h to 0.2 h, the results sufficiently converge on the “true” solution for the filtered velocity field; that is, the time step is sufficiently shorter than the Lagrangian decorrelation time for the filtered velocities to yield an accurate result. This justifies the use of a time step of 0.2 h in the float-tracking algorithm described in Hinckley *et al.* (1996).

Fewer of the float tracks cross into shallow shelf areas when filtered velocities are used, compared to the unfiltered technique. This deficiency could be addressed to some extent by adding a suitable random walk component to the tracked floats, an equivalence first noted by Taylor (1921). We caution, however, that the diffusivity lost by temporal filtering may be spatially dependent, and that spatial variation in the magnitude

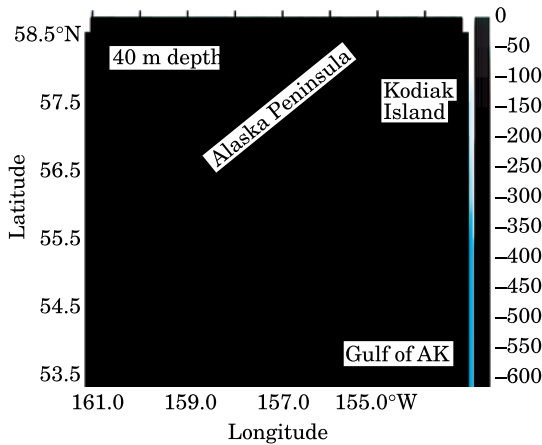


Figure 9. Tracks of floats that were constrained to remain at 40 m depth, generated by directly updating float positions at each time step (SPEM simulation for 1987; further as in Figure 7).

of a random walk can pose special difficulties (Hunter *et al.*, 1993; Holloway, 1994).

Hinckley *et al.* (1996) noted the importance of vertical position in determining the paths of individuals. Figure 9 underscores this point by showing float paths as in case c, but with all floats constrained to remain at 40 m depth, rather than being free to follow the flow field in three dimensions. The influence of the eddy field is markedly reduced by this constraint; floats do not circulate around the eddy pair as they did in other cases.

Coupled run output, timing, and storage

Some illustrative results from the coupled SPEM-IBM-NPZ models for mid-June, 1987 are shown in Figure 10: (a) shows a cyclonic eddy located in the deepest part of the sea valley (near 56.5°N–156°E), (b) shows the total numbers of all copepodite stages of *Pseudocalanus* (the food resource of larval pollock), and (c) shows the positions of 1600 individual fish released (with mortality set to zero), shaded according to length. The individual lengths vary, owing to the different prey fields encountered during their life history; larvae >8-mm ingest a mixture of nauplii and copepodites. A cluster of medium-sized larvae (8–16 mm) is trapped within the eddy. A tongue of low zooplankton concentration is being advected around the southern rim of the eddy, and shorter fish are associated with that feature. A tongue of higher zooplankton concentration, advecting around the northern rim of the eddy, has fewer but generally longer fish associated with it. Regions downstream and shoreward of this feature also exhibit greater lengths.

While some patchiness of fish size can be produced through purely kinematic effects related to the time of spawning (e.g. a cluster of late-spawned, smaller individuals trapped in an eddy), clearly the spatially variable

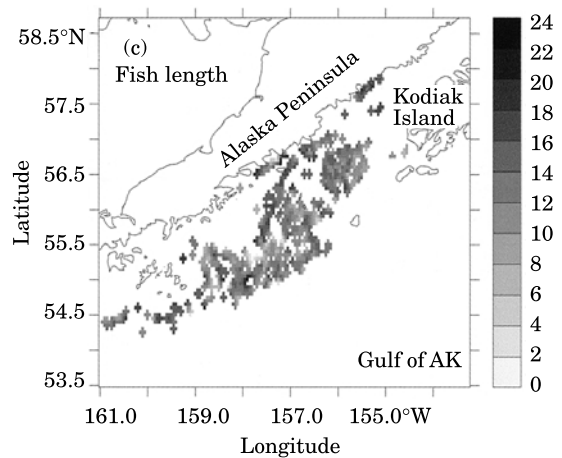
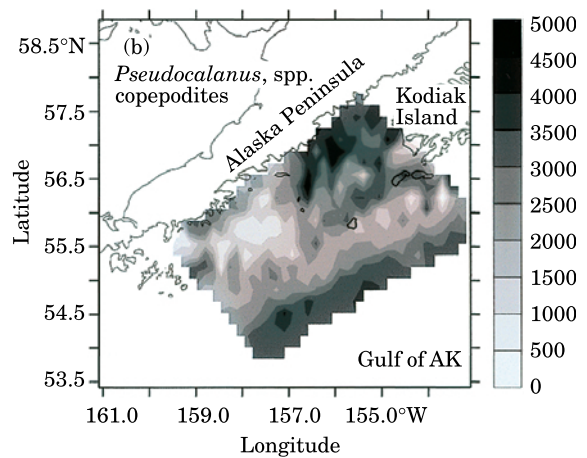
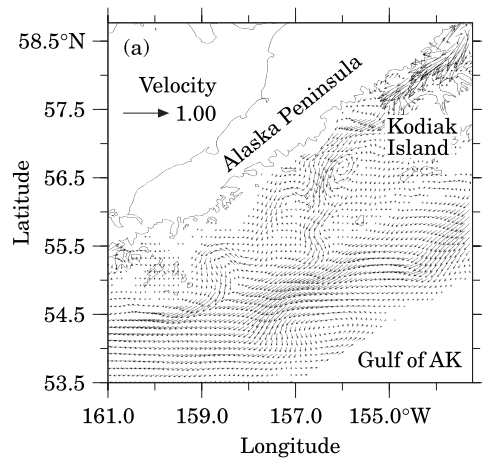


Figure 10. Model output for mid-June, 1987: (a) SPEM (surface velocity in m s^{-1}); (b) NPZ (shading: total concentration of all copepodite stages of *Pseudocalanus* spp. in the mixed layer; number m^{-3}); and (c) IBM (positions of individual pollock shaded by length in mm).

Table 1. Statistics for the three coupled models.

Model type	SPEM	NPZ	IBM
Model size	257'97'9 grid	20'20'100 grid	1600 ind.
Resolution horizontal (km)	4	20	4
Vertical (m)	5	1	5
Daily output	Velocity Salinity Temperature	Nitrate concentration Phytoplankton biomass Zooplankton biomass (14 stages/species)	Length Weight Position
Simulation time (model days)	270	95	210
Output file (gbytes)	1.0	0.5	0.02
Execution time ¹ (CPU-h)	125	5	5

¹On CRAY Y-MP.

prey field contributes to the patchiness of fish attributes in this model. The use of a dynamic prey field also results in different mean growth and survival for groups of individuals spawned at different places and times (Hinckley *et al.*, this volume).

All model results described were generated using a CRAY Y-MP vector processing supercomputer. Statistics of runs and output files are listed in Table 1. The physical model consumes the largest amount of computer time. Indeed, this is the primary motivation for decoupling the physical and biological runs, because this allows for much more testing and sensitivity analysis of the biological models. The output files from the physical model, while large, are not prohibitively so, and can be transferred to local workstations for detailed analysis and plotting. Statistics of the IBM are dependent on the number of individuals followed.

Conclusions

Spatially explicit biophysical models, spanning multiple trophic levels, can be a powerful tool for probing hypotheses about the early life history of marine fish. Throughout our ongoing work with coupled hydrodynamic, population, and trophodynamic models, we have attempted to balance desirable features with practical limits on computing power. Our experience thus far has led to the following conclusions. (1) Storage of pre-filtered and decimated model velocity and scalar fields, for later use by Lagrangian biological models, is both feasible and efficient. Supercomputing platforms with reasonable large (several gigabyte) storage capacity are necessary for much of this work (but individual workstations now have the required speed and storage capabilities for many simulations). (2) The results are reasonably accurate given a sufficiently small time step for spatial tracking; however, care must be taken to consider the information lost through filtering. Practical techniques exist to recover some of the lost information, such as tides. (3) Spatially varying prey fields, derived using a traditional Eulerian approach, can be applied

in a straightforward manner to spatially explicit (Lagrangian) IBMs, and should typically enhance the variance of individual attributes. (4) Boundary conditions for Eulerian prey models should benefit from a careful use of data assimilation when field data are available.

As our models evolve to greater complexity, there is a continuing need for calibration and sensitivity analyses of the coupling methods for linking information. For example, there is a strong need for further sensitivity analyses of grid spacing in the NPZ model. Equally important is the need for further comparison of three-dimensional NPZ model output with chlorophyll and zooplankton data. For chlorophyll, satellite-derived estimates may be useful for comparing at least broad spatial patterns, and possibly higher-order spatial statistics, with those produced from the model.

Acknowledgements

This is contribution no. 1920 from NOAA/ Pacific Marine Environmental Laboratory, contribution no. 318 to NOAA's Fisheries Oceanography Coordinated Investigations, and contribution no. 475 from the Joint Institute for the Study of the Atmosphere and Oceans (JISAO) under NOAA cooperative agreement no. NA67RJ0155.

© 2001 US Government

References

- Crowder, L. W., Rice, J. A., Miller, T. J., and Marschall, E. A. 1993. Empirical and theoretical approaches to size-based interactions and recruitment variability in fishes. *In* Individual-Based Models and Approaches in Ecology, pp. 237–255. Ed. by D. DeAngelis, and L. Gross. Chapman and Hall, London. 525 pp.
- DeAngelis, D. L., Godbout, L., and Shuter, B. J. 1991. An individual-based approach to predicting density-dependent dynamics in smallmouth bass populations. *Ecological Modelling*, 57: 91–115.

- Frost, B. W. 1987. Grazing control of phytoplankton stock in the open subarctic Pacific Ocean: a model assessing the role of mesozooplankton, particularly the large calanoid copepods *Neocalanus* spp. *Marine Ecology Progress Series*, 39: 49–68.
- Frost, B. W. 1993. A modelling study of processes regulating plankton standing stock and production in the open subarctic Pacific Ocean. *Progress in Oceanography*, 32: 17–56.
- Fukumori, I., and Malanotte-Rizzoli, P. 1995. An approximate Kalman filter of ocean data assimilation: an example with an idealized Gulf Stream model. *Journal of Geophysical Research*, 100: 6777–6793.
- Haidvogel, D. 1982. On the feasibility of particle tracking in Eulerian ocean models. *Ocean Modelling*, 45: 4–9.
- Haidvogel, D. B., Wilkin, J. L., and Young, R. 1991. A semi-spectral primitive equation ocean circulation model using vertical sigma and orthogonal curvilinear coordinates. *Journal of Computational Physics*, 94: 151–185.
- Hermann, A. J., and Stabeno, P. J. 1996. An eddy resolving model of circulation on the western Gulf of Alaska shelf. I. Model development and sensitivity analyses. *Journal of Geophysical Research*, 101: 1129–1149.
- Hermann, A. J., Hinckley, S., Megrey, B. A., and Stabeno, P. J. 1996. Interannual variability of the early life history of walleye pollock near Shelikof Strait, as inferred from a spatially explicit, individual-based model. *Fisheries Oceanography*, 5 (suppl. 1): 39–57.
- Hillgruber, N., Haldorson, L. J., and Paul, A. J. 1995. Feeding selectivity of larval walleye pollock *Theragra chalcogramma* in the oceanic domain of the Bering Sea. *Marine Ecology Progress Series*, 120: 1–10.
- Hinckley, S. 1999. Biophysical mechanisms underlying the recruitment process in walleye pollock (*Theragra chalcogramma*). PhD Dissertation, University of Washington, Seattle. 258 pp.
- Hinckley, S., Hermann, A. J., and Megrey, B. A. 1996. Development of a spatially explicit, individual-based model of marine fish early life history. *Marine Ecology Progress Series*, 139: 47–68.
- Hinckley, S., Hermann, A. J., Meir, K. L., and Megrey, B. A. 2001. Importance of spawning location and timing to successful transport to nursery areas: a simulation study of Gulf of Alaska walleye pollock. *ICES Journal of Marine Science* doi:10.1006/jmsc.2001.1096.
- Hoffmann, E. E., Hedstrom, K. S., Moisan, J. R., Haidvogel, D. B., and Mackas, D. L. 1991. The use of simulated drifter tracks to investigate general transport patterns and residence times in the coastal transition zone. *Journal of Geophysical Research*, 96: 15 041–15 052.
- Holloway, G. 1994. On modeling vertical trajectories of phytoplankton in a mixed layer. *Deep-Sea Research (Part 2, Topical Studies in Oceanography)*, 41: 957–959.
- Hunter, J. R., Craig, P. D., and Phillips, H. E. 1993. On the use of random walk models with spatially variable diffusivity. *Journal Computational Physics*, 106: 366–376.
- Incze, L. S., and Ainaire, T. 1994. Distribution and abundance of copepod nauplii and other small (40–300 μm) zooplankton during spring in Shelikof Strait, Alaska. *Fishery Bulletin*, 92: 67–78.
- Incze, L. S., Siefert, D. W., and Napp, J. M. 1997. Mesozooplankton of Shelikof Strait, Alaska: abundance and community composition. *Continental Shelf Research*, 17: 287–305.
- Kendall, A. W. Jr, Clarke, M. E., Yoklavich, M. M., and Boehlert, G. W. 1987. Distribution, feeding, and growth of larval walleye pollock, *Theragra chalcogramma*, from Shelikof Strait, Gulf of Alaska. *Fishery Bulletin US*, 85: 499–521.
- Kendall, A. W. Jr, Schumacher, J. D., and Kim, S. 1996. Walleye pollock recruitment in Shelikof Strait: applied fisheries oceanography. *Fisheries Oceanography*, 5 (suppl. 1): 4–18.
- Lande, R., and Lewis, M. R. 1989. Models of photoadaptation and photosynthesis by algal cells in a turbulent mixed layer. *Deep-Sea Research*, 36: 1161–1175.
- MacKenzie, B. R., and Leggett, W. C. 1993. Wind-based models for estimating the dissipation rates of turbulent energy in aquatic environments: empirical comparisons. *Marine Ecology Progress Series*, 94: 207–216.
- Megrey, B. A., and Hinckley, S. 2001. The effect of turbulence on feeding of larval fishes: a sensitivity analysis using an individual based model. *ICES Journal of Marine Science* doi:10.1006/jmsc.2001.1104.
- Nakatani, T., and Maeda, T. 1987. Distribution and movements of walleye pollock larvae *Theragra chalcogramma* in Funka Bay and the adjacent waters. *Hokkaido Bulletin of Japan Society of Scientific Fisheries*, 53: 1583–1591.
- Napp, J. M., Incze, L. S., Ortner, P. B., Siefert, D. L. W., and Britt, L. 1996. The plankton of Shelikof Strait, Alaska: standing stock, production, mesoscale variability and their relevance to larval fish survival. *Fisheries Oceanography*, 5 (suppl. 1): 19–38.
- Rose, K. A., Christensen, S. W., and DeAngelis, D. L. 1993. Individual-based modeling of populations with high mortality: a new method for following a fixed number of model individuals. *Ecological Modelling*, 68: 273–292.
- Royer, T. C. 1982. Coastal freshwater discharge in the north-east Pacific. *Journal of Geophysical Research*, 87: 2017–2021.
- Schumacher, J., and Kendall, A. W. Jr 1995. An example of fisheries oceanography: Walleye pollock in Alaskan waters. U.S. National Report to International Union of Geodesy and Geophysics 1991–1994. *Reviews of Geophysics, Suppl.*, 33: 1153–1163.
- Stabeno, P. J., and Hermann, A. J. 1996. An eddy resolving model of circulation on the western Gulf of Alaska shelf. 2. Comparison of results to oceanographic data. *Journal of Geophysical Research*, 101: 1151–1161.
- Stabeno, P. J., Hermann, A. J., Bond, N. A., and Bograd, S. J. 1995. Modeling the possible impact of climate change on the survival of larval walleye pollock (*Theragra chalcogramma*) in the Gulf of Alaska. *Canadian Special Publication in Fisheries and Aquatic Sciences*, 121: 719–727.
- Taylor, G. I. 1921. Diffusion by continuous movements. *Proceedings of the London Mathematical Society (Series 2)*, 10: 196–212.
- Werner, F. E., et al. 1993. Influences of mean advection and simple behavior on the distribution of cod and haddock early life stages on Georges Bank. *Fisheries Oceanography*, 2: 43–64.
- Werner, F. E., Perry, R. I., Lough, R. G., and Naimie, C. E. 1996. Trophodynamic and advective influences on Georges Bank larval cod and haddock. *Deep-Sea Research (Part 2, Topical Studies in Oceanography)*, 43: 1793–1822.
- Woods, J., and Barkmann, W. 1993. Diatom demography in winter – simulated by the Lagrangian Ensemble method. *Fisheries Oceanography*, 2: 202–222.